Joule

CellPress

Report

The Thermal Stability of Lithium Solid Electrolytes with Metallic Lithium

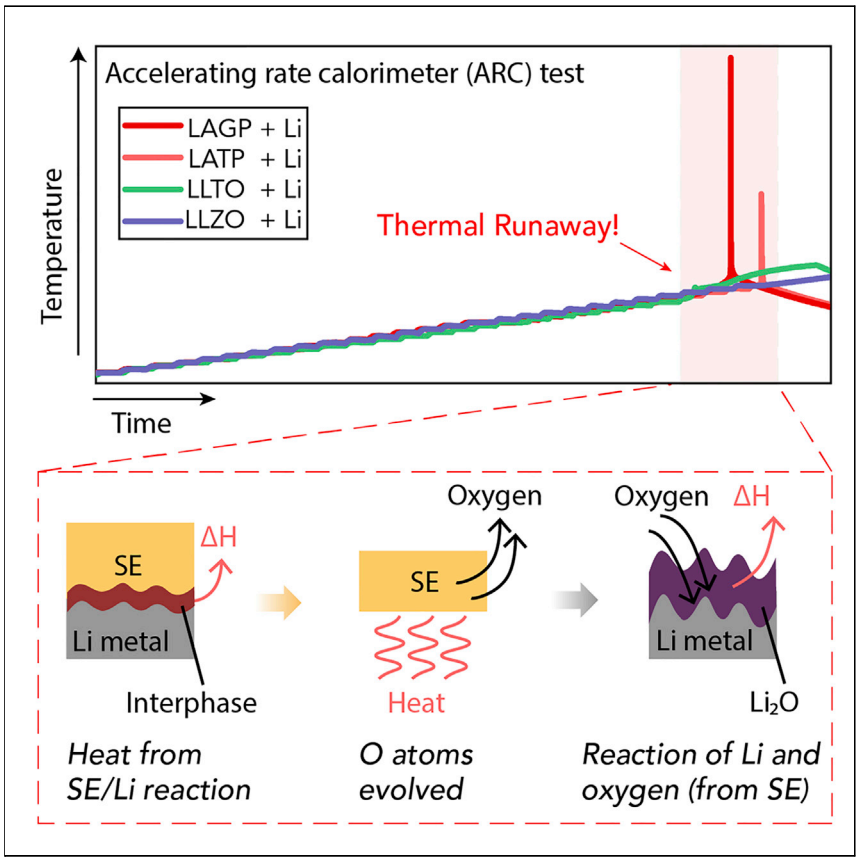

This study quantifies the thermal stability of oxide SEs with Li metal and observes thermal runaway behaviors of common SEs with Li metal. Theoretic calculations and experiments indicate that the oxygen generation from the SEs at elevated temperatures triggers a highly exothermic reaction with molten metallic Li, leading to thermal runaway. As an alert to the community, our results highlight the urgency to systematically investigate and deepen the understanding of safety issues in ASSBs.

Rusong Chen, Adelaide M. Nolan, Jiaze Lu, ..., Liquan Chen, Xuejie Huang, Hong Li

xyu@iphy.ac.cn (X.Y.)
yfmo@umd.edu (Y.M.)
hli@iphy.ac.cn (H.L.)

HIGHLIGHTS

The thermal stabilities of four prevalent SEs with Li were elucidated and compared

Theoretical calculations reveal activation on oxygen of SE when contacting with Li

Oxygen generation and the subsequent reaction with Li lead to the thermal runaway

Interfacial properties affect the thermal stability between SE and Li

Chen et al., Joule 4, 812–821
April 15, 2020
https://doi.org/10.1016/j.joule.2020.03.012

Joule

CellPress

Report

The Thermal Stability of Lithium Solid Electrolytes with Metallic Lithium

Rusong Chen,[1,2] Adelaide M. Nolan,[3] Jiaze Lu,[1,2] Junyang Wang,[1,2] Xiqian Yu,[1,2,4,*] Yifei Mo,[3,*] Liquan Chen,[1] Xuejie Huang,[1] and Hong Li[1,2,4,5,*]

SUMMARY

All-solid-state lithium-metal batteries are regarded as promising next-generation battery systems. While thermal runaway in conventional Li-ion batteries is known to cause safety hazards, the thermal issues posed by highly reactive metallic lithium (Li) with non-flammable ceramic solid electrolytes (SEs) have been less studied but are critical for the safety of all-solid-state Li-metal batteries. Here, we quantify the thermal stability of four prevalent oxide SEs with metallic Li using the accelerating rate calorimeter (ARC). Thermal runaway is observed during ARC tests for four widely used SEs when contacting with Li, while no obvious heat releases from garnet with Li. The oxygen generation from SEs at elevated temperatures is found to be responsible for the thermal runaway with Li. Our results indicate potential safety issues in all solid-state batteries (ASSBs) brought by highly reactive metallic Li and oxygen from SEs at increased temperatures, emphasizing the need for investigating thermal safety issues in ASSBs.

INTRODUCTION

Lithium-ion batteries (LIBs) have been the dominant energy storage devices for powering electric vehicles (EVs).[1] In order to achieve higher energy density batteries, Li-metal batteries employing Li-metal anode would deliver higher energy density than current LIBs, as the Li-metal anode exhibits high specific capacity and low potential.[2,3] However, Li dendrite growth and the resulting internal short circuit remain major concerns and are grand safety challenges for Li-metal batteries. While intensive effort has been undertaken to understand the dendrite growth mechanisms and solve the dendrite growth problems, the safety issues posed by the highly reactive metallic Li are less investigated and their mechanisms are far less understood. Metallic Li is highly reactive and the reaction can generate a significant amount of heat during the battery failure.[4,5] For these reasons, investigations of the safety issues associated with highly reactive Li metal are a high priority for the large-scale application of Li metal batteries.

All-solid-state batteries (ASSBs) replace the flammable liquid organic electrolytes with thermally stable inorganic ceramic solid electrolytes (SEs)[6] and so are commonly regarded as compatible with Li-metal anode with good safety. While there have been numerous efforts investigating the chemical and electrochemical stability between SE/Li interfaces to improve cell performance of ASSBs,[7–10] the thermal issues of SE materials combined with Li-metal anode under high temperature are less studied.[11] Kang et al.[12] studied the thermal failure behavior on $Li_{1.5}Al_{0.5}Ge_{1.5}(PO_4)_3$ (LAGP)/Li interface and reported that thermal runaway happened after the LAGP pellet made contact with molten Li. Later investigations

Context & Scale

Countless applications for lithium-ion batteries (LIBs) have been plagued by safety issues, especially in electronic vehicles. To meet increasing demand for ever higher energy density and resolve safety issues, all-solid-state batteries (ASSBs) utilizing thermally stable inorganic solid electrolytes (SEs) to enable Li-metal anode have been widely pursued. However, the introduction of Li metal may bring additional safety concerns because of Li dendrite growth and the high reactivity of Li. So far, the safety performance and the safety limits of ASSBs remain largely unknown, and therefore should be systematically studied before practical application. This study observes and quantifies the thermal stability of oxide SEs with Li metal, indicating potential safety issues in SE materials with metallic Li. Given the crucial role of the thermal stability of material components for overall battery safety, the results highlight the importance and urgency for safety investigations of ASSBs.

reported that cracks and expansions occurred between NASICON SE with metallic Li,[13,14] while the thermal failure was not observed at the Li/Garnet interface,[15] indicating that different SEs exhibit distinct thermal behaviors in contact with metallic Li. Since thermal stability of SEs against metallic Li plays a key role in the safety of ASSBs, a quantitative and systematic understanding about the thermal behavior of SEs in the presence of highly reactive metallic Li is urgently needed.

In this work, we utilize the accelerating rate calorimeter (ARC), a technique widely employed in quantifying the safety of commercial LIBs,[16] to elucidate the thermal stability of the four prevalent SEs, NASICON-type LAGP, $Li_{1.4}Al_{0.4}Ti_{1.6}(PO_4)_3$ (LATP), perovskite-type $Li_{3x}La_{2/3-x}TiO_3$ (LLTO), and garnet-type $Li_{6.4}La_3Zr_{1.4}Ta_{0.6}O_{12}$ (LLZO) with metallic Li. The ARC tests found that thermal runaway occurred in LAGP, LATP, and LLTO, contacted with Li metal, while no obvious heat generation occurred in LLZO with Li. By comparing the onset temperature and the heat-generation rate of different material systems, the thermal stability versus Li of the four SEs was identified to follow the order of LAGP < LATP < LLTO < LLZO. In addition, the underlying mechanism of the thermal runaway of the SE-Li sample was revealed by the thermodynamic analyses, based on first principles calculations. The oxygen release from the SEs at elevated temperatures triggers a highly exothermic reaction with molten metallic Li, leading to thermal runaway. Our work quantifies the thermal stability of the oxide SEs with metallic Li at the materials level and uncovers potential safety issues posed by the high reactivity of metallic Li with oxide SEs. This study highlights the urgency of investigating the thermal-related safety issues of ASSBs.

RESULTS

Experimental Demonstration

The ARC test procedure is illustrated in Figure 1A. Different SE powders were sandwiched with metallic Li foils and sealed in pouch bags respectively, which were attached with a high accuracy thermocouple in the ARC chamber. The samples were heated to an elevated temperature with a temperature increment of 10°C under the heat-wait-seek testing mode (HWS mode; Figures 1B and S1). Between temperature increments, the sample was held for 30 min to stabilize the temperature. Then the seeking mode operates, if the notable self-heating behavior was detected (self-heating temperature increasing rate > 0.02°C/min in a seeking period, the onset temperature is denoted as T_1), the HWS mode would be stopped and the temperature of the chamber would be kept the same as the sample to provide an adiabatic environment until the temperature exceeds the upper limit of the temperature range (30°C–350°C). Otherwise, another HWS mode begins. A typical ARC test curve of LIBs is shown in Figure 1C. Three characteristic temperatures, T_1, T_2, and T_3[17,18] provide a quantitative description of the safety performance. T_1 is the onset temperature of the notable self-heating reactions. T_2 is the initial temperature at which thermal runaway occurs, and the severe thermal hazard cannot be avoided once the temperature surpasses T_2. Although controversy about T_2 remains, here, we define T_2 as the temperature where the self-heating rate reaches 60°C/min (1°C/s).[17] T_3 is the maximum temperature of the sample during the whole test processes, reflecting the energy release during thermal runaway. In this study, although the ARC experiments were performed with SE/Li materials rather than solid-state batteries, these characteristic temperatures are utilized to represent the ARC results.

Materials characterizations and pre-treatments were performed on SEs to identify their phases and surface chemical states, and thus to establish reliable correlations between SEs and the ARC test results (Figures S2 and S3). As detailed in the

[1]Beijing Advanced Innovation Center for Materials Genome Engineering, Key Laboratory for Renewable Energy, Beijing Key Laboratory for New Energy Materials and Devices, Institute of Physics, Chinese Academy of Sciences, Beijing 100190, China

[2]Center of Materials Science and Optoelectronics Engineering, University of Chinese Academy of Sciences, Beijing 100049, China

[3]Department of Materials Science and Engineering, University of Maryland, College Park, MD 20742, USA

[4]Yangtze River Delta Physics Research Center Co. Ltd., Liyang 213300, China

[5]Lead Contact

*Correspondence: xyu@iphy.ac.cn (X.Y.), yfmo@umd.edu (Y.M.), hli@iphy.ac.cn (H.L.)

https://doi.org/10.1016/j.joule.2020.03.012

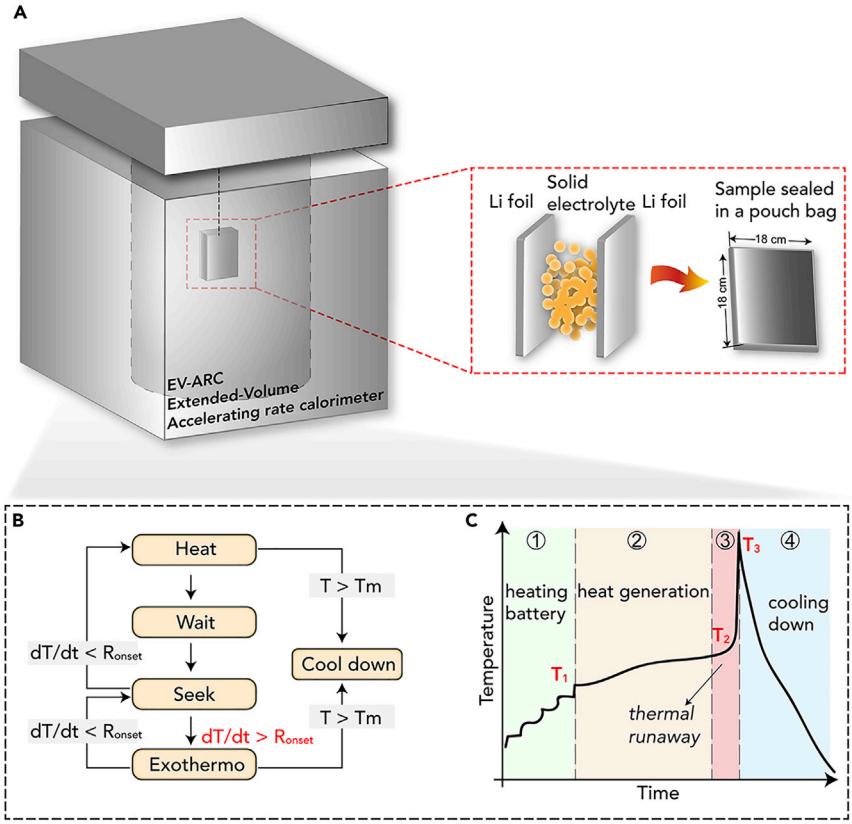

Figure 1. Experimental Demonstration

(A) Schematic illustration of method for testing thermal stability of SEs against metallic Li. SE powders were sandwiched with Li foils and vacuum-sealed in an aluminum plastic pouch bag.

(B) Heat-wait-seek (HWS) operating mode of ARC, where the R_{onset} is the set as 0.02°C/min, and the Tm (maximum test temperature) is set to be 350°C.

(C) A typical ARC test curve of a commercial pouch-type LIB. Three characteristic temperatures quantify the thermal stability of the samples, as T_1 refers to the self-heating onset temperature, T_2 is the critical temperature of thermal runaway, and T_3 indicates the highest temperature of the sample during thermal runaway. The lower the temperatures T_1 and T_2, the easier for a battery thermal runaway to happen, and the higher T_3 illustrate the higher heat release and worse safety performance of the battery during thermal runaway.

Supplemental Information, the mass composition of all the SE/Li samples are kept nearly the same, as shown in Table S1. An 850°C calcination was applied for LLTO and LLZO to remove the surface absorbed Li_2CO_3 (Figure S3; Tables S2 and S3).[19–21] For LAGP and LATP powders, which are chemically stable in air,[22] 120°C/5 h treatment was performed to remove the potentially absorbed water.

ARC Results of Different SE/Li Samples

Figure 2 displays the ARC results of the four SE/Li systems. It was found that LAGP/Li, LATP/Li, and LLTO/Li show obvious temperature increases during the ARC test, while LLZO/Li sample exhibits no significant heat generation. The sharp temperature spike and high temperature increasing rate (>1,000°C /min) for LAGP and LATP contained samples indicates a severe thermal runaway process (Figures 2A–2D). Despite a small amount of heat release observed at ~290°C in LLZO/Li, the maximum self-heating rate is 0.675°C/min (Figures 2G and 2H), indicating that the thermal hazard cannot occur for LLZO/Li sample at high temperature. Besides, LLZO/Li and pure Li samples yield similar ARC test results (Figure S4), so the small amount of heat

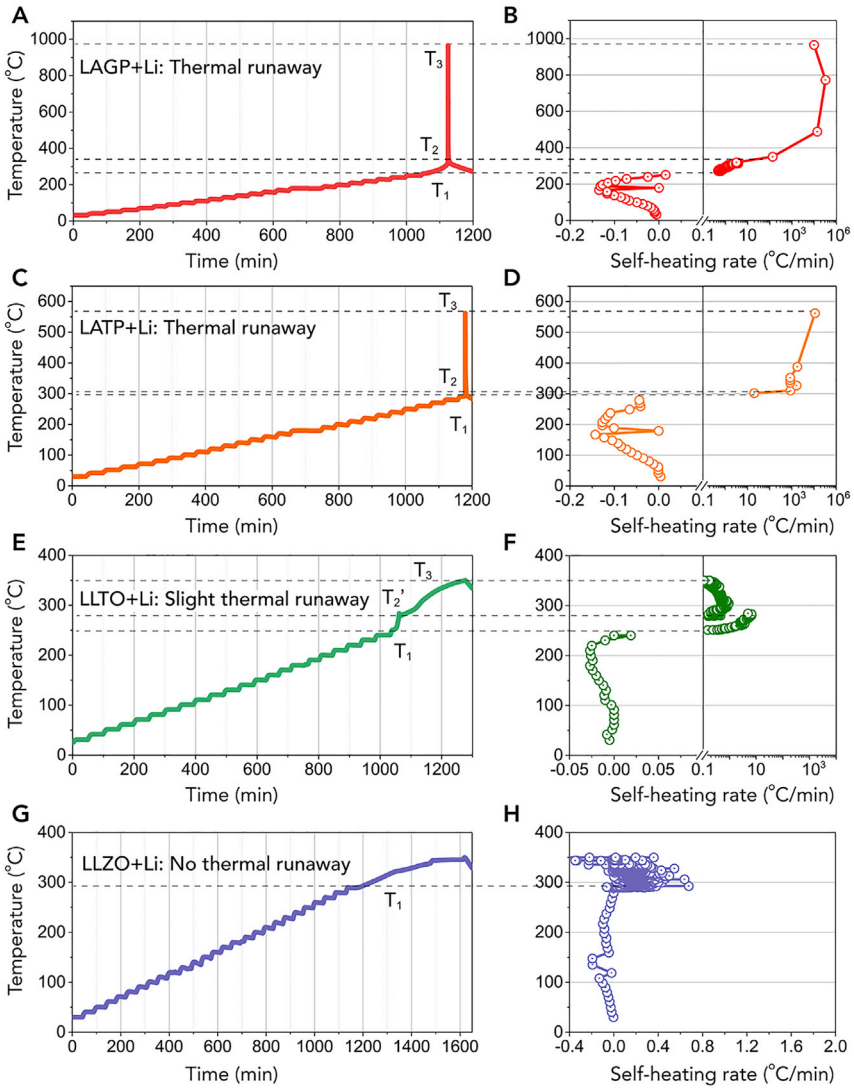

Figure 2. ARC Test Results of Four SE/Li Samples

(A, C, E, and G) Images showing the time-dependent temperature curves of LAGP/Li (A), LATP/Li (C), LLTO/Li (E), and LLZO/Li (G).

(B, D, F, and H) illustrate the temperature as the function of self-heating rate of LAGP/Li (B), LATP/Li (D), LLTO/Li (F), and LLZO/Li (H).

The sharp temperature increment of the LAGP and LATP samples reveals the occurrence of thermal runaway, as indicated between T_2 and T_3 in (A)–(D). The relative slower heat release from the LLTO sample is also highlighted in (E) and (F). The LLZO/Li sample displays nearly the same thermal behavior as pure Li sample, indicating no heat generated from LLZO/Li interface as shown in (G) and (H). Note that the T_1 was recorded by the equipment by monitoring the self-heating rate. When self-heating rate reached 0.02°C/min, the "heat-seek-wait" mode was stopped and the temperature of the chamber was kept the same as the sample to provide an adiabatic environment.

generation at around 290°C may be attributed to the slight reactions between aluminum plastic film and Li. In addition, no new heat releasing behavior was observed with the addition of LLZO, illustrating the high thermal stability between LLZO and Li. As for the LLTO/Li sample, the notable temperature increase between 250°C and 280°C indicates the occurrence of heat-generation reactions, although the rate of increase of the temperature is relatively low (~10°C/min, denoted as

Table 1. Key Parameters Extracted from the ARC Test Results of Different SE/Li Samples

Materials	T_1 (°C)[a]	T_2 (°C)[b]	T_3 (°C)[c]	Δt (min)[d]	dT/dt Max[e] (°C/min)	ΔT (°C)[f]
LATP + Li	290.619	301.725	561.827	7.540	11,083.623	271.208
LAGP + Li	261.939	320.428	966.190	70.242	32,076.152	704.251
LLTO + Li	251.147	256.198	350.006	7.999	6.584	98.859
LLZO + Li	292.920	//[g]	//[g]	//[g]	0.675	//[g]

[a]T_1 represents the onset temperature of the sample self-heating reactions, defined as the temperature increasing rate, exceeds 0.02°C/min.
[b]T_2 is the onset temperature where the heating rate exceeds 60°C/min. For LLTO/Li sample, the T_2 is defined as the temperature where the heating rate reaches to the maximum value.
[c]T_3 is the highest temperature of the sample during the whole test process.
[d]Δt is the process time of the sample from T_1 to T_2.
[e]dT/dt max represents the maximum self-heating rate of the samples during ARC test.
[f]$\Delta T = T_3 - T_1$, refers to the temperature increment of the sample during thermal runaway.
[g]Since no obvious heat release was observed on LLZO/Li sample, the characteristic parameters for LLZO sample are not taken into account to evaluate their thermal behaviors.

T_2'). As the critical temperature increasing rate of a thermal runaway process is defined as 60°C/min, we characterize the heat-generation behavior of LLTO/Li sample as "slight thermal runaway" to distinguish it from LLZO/Li samples, which show no notable heat release. The above results show that the SEs in the order LLZO, LLTO, LATP, and LAGP exhibit decreasing thermal stability against metallic Li, which is well supported by the digital pictures of the samples after the ARC tests (Figure S5). The test pouches of LAGP and LATP were totally broken down, while the LLZO sample maintained its pristine morphology without breaking, indicating the high thermal stability between LLZO and Li, in agreement with previously reported results.[23] Besides, it should be noted that the thermal runaway behavior of the SEs/Li is distinct with that of traditional LIBs, where a longer time is often taken from T_1 to T_2 (Figure 1C). As the present study mainly focuses on SE/Li interfaces, such differences may be attributed to a series of chain reactions, including solid electrolyte interphase (SEI) decomposition, separator melting, electrolyte evaporation, internal short circuit, etc., that happen in LIBs during temperature elevation, and it may take several hours to reach T_2 after self-heating begins.[16,24]

For a better understanding of the differences in thermal behavior between different SEs and Li, Table 1 compares the key parameters extracted from the ARC test results. The self-heating rate for LAGP/Li and LATP/Li samples reaches 32,076.152°C/min and 1,1083.623°C/min, respectively, which is much higher than that for LLTO and LLZO samples, respectively. Moreover, although these three samples exhibit similar T_1 and T_2 values (Figure S6), LAGP exhibits a much higher T_3, leading to a high ΔT. As the three samples have almost the same chemical mass composition (Table S1), the heat capacity (C_p) can be regarded as the same for the three samples, and thus ΔT can reflect the heat generation of the samples during thermal runaway process, based on $\Delta H = M \cdot C_p \cdot (T_3 - T_1)$, where M is the sample mass. The highest heat release of LAGP/Li sample was also revealed by the thermal runaway experiments performed in an air-filled glove box (Videos S1, S2, and S3). The heat generated from the LAGP/Li thermal runaway is high enough to melt stainless steel (Figure S7). The thermal stability of the four SEs with Li metal follows the order of LLZO > LLTO > LATP > LAGP, and is consistent with the thermodynamic analyses shown in the next subsection.

Thermodynamic Calculations and Post-reaction Analysis

Theoretical analyses were performed to understand the origin of the thermal runaway phenomena of SEs with metallic Li. First, the interface stability caused by

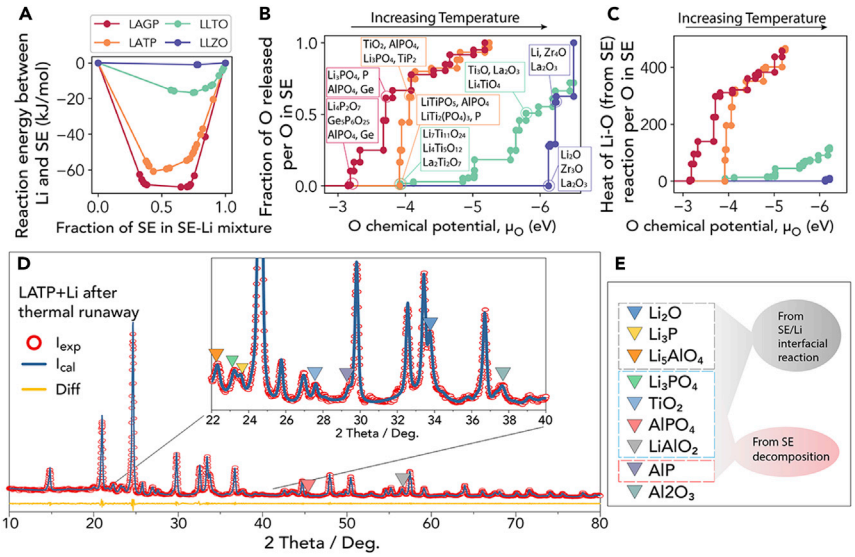

Figure 3. Thermodynamic Analyses of SE with Metallic Li from First Principles Calculations and Post-Reaction XRD Analysis

(A) The mutual reaction energy per mole fraction of SE between the SE materials and Li metal at different mixing ratios of Li and SE. The mutual reaction energy between the Li and SE of the Li-SE mixture. The energies were normalized to per mol of the Li-SE mixture.

(B) Thermodynamic profiles of oxygen evolution as a function of O chemical potential and temperature for SE materials. The oxygen release from each SE was normalized to the O content in the SE.

(C) The generated heat in reaction of metallic Li with oxygen released from the SE. The energies were normalized to the mole fraction of O released from the SE.

(D) Post-reaction XRD analysis of the reaction products after LATP/Li thermal runaway.

(E) The detected phases and their assignments with LATP/Li interfacial reaction and LATP decomposition.

the chemical reactions between SE and metallic Li was examined by the thermodynamic scheme based on density functional theory (DFT) calculations.[25–27] The SE/Li samples were modeled as a pseudo-binary of two materials, and the mutual reaction energy between the materials to form thermodynamically favorable phase combinations was calculated as a function of mixing ratio (Figure 3A; Tables S4–S8). Among these SEs, LATP and LAGP are highly reactive with Li metal, with decomposition energies of over −60 kJ/mol of SEs and Li, while LLZO is almost thermodynamically stable with Li metal within typical DFT errors.[28] Although the interfacial reaction is thermodynamically favorable, we expect it is not the key mechanism causing thermal runaway observed in ARC test. Significant flame can be observed during the thermal runaway of SE/Li sandwich even in an argon (Ar) filled environment (O_2 < 0.1, H_2O < 0.1 ppm; Videos S1, S2, and S3) without the fire supporting gas. Thus, the SE/Li interfacial reactions are inadequate to initiate a thermal runaway.

Using the grand canonical phase diagram scheme developed by Ceder and coworkers[29–31] quantifying the thermal runaway in cathode materials, we evaluated the thermodynamic profile of oxygen evolution from these SE materials (Figure 3B; Tables S9–S12) as a function of the decrease of the oxygen chemical potential, which corresponds to the increase of temperature (Experimental Procedures). Our results (Figure 3B) indicate that LAGP and LATP have the lowest onset (i.e., lowest temperatures) of favorable O_2 release, followed by LLTO. Among all these materials, LLZO exhibits the highest onset (i.e., highest temperature) of O_2 release, suggesting the best stability and lack of thermal runaway of LLZO. The calculated trend of oxygen

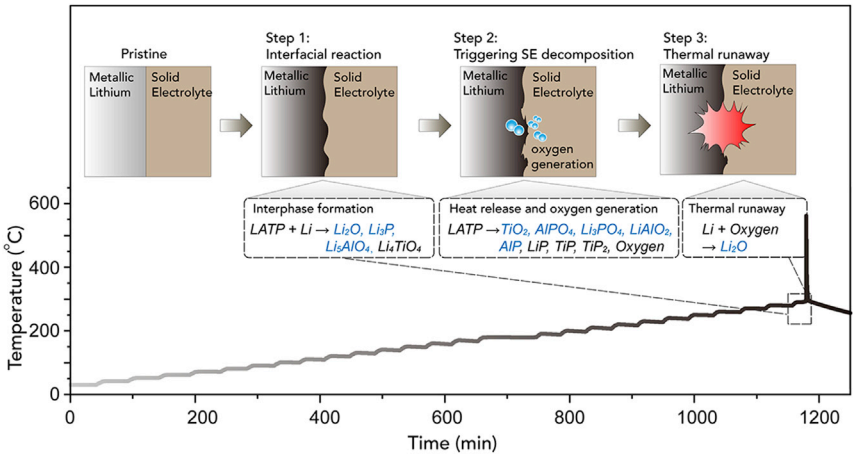

Figure 4. Schematic Illustration of Multi-step Thermal Runaway Reaction between SEs and Metallic Li

The LATP here is referred as an example, the products marked by blue were detected in this study.

release of the SEs follows LAGP > LATP > LLTO > LLZO, in agreement with our ARC experiment observations.

The potential release of oxygen from the SE can greatly promote the reaction with molten Li metal, leading to thermal runaway. From our calculations, LAGP releases a large amount of oxygen within a small range of temperature increase, suggesting a large thermal runaway and high temperature achieved, and LATP shows similar behavior. LLTO needs a larger temperature increase to release a decent amount of oxygen, and LLZO is stable until a significantly higher temperature. Furthermore, the reaction energy of the released oxygen from SE with the molten Li is calculated (Figure 3C), and oxygen release onset and heat generated follows the trend of LAGP > LATP > LLTO > LLZO, all agreeing with ARC experiment observations.

Moreover, the reaction products of both the SE/Li interfacial reactions and SE decompositions were identified in the refined post-reaction XRD analysis of the residue of SE/Li after thermal runaway (LATP as an example in Figure 3D). The reaction products (Figure 3E; Table S13), such as AlP were observed as characteristic products from LATP decomposition, Li_3P, Li_2O, and Li_5AlO_4 were identified from LATP/Li interfacial reactions, and the observed Li_3PO_4, TiO_2, $AlPO_4$, and $LiAlO_2$ could be the products from both LATP/Li interfacial reaction and LATP decomposition (Figures 3D and 3E).The results of other SEs can be seen in Figures S8 and S9 and Tables S14 and S15. While the thermodynamics suggest O_2 gas generation accompanied the decomposition of SE, no free O_2 gas was detected in experiments (Figure S10). In the experiments, the highly reactive metallic Li may directly react with the oxygen from SE activated by the increased temperature without the step of O_2 gas generation.[32] Even though no O_2 gas was directly detected in the present report, the post-reaction XRD analysis indicated that both the SE/Li interfacial reaction and SE decomposition were involved in thermal runaway, confirming the theoretical prediction of the thermal decomposition process of SEs and the subsequent reactions of oxygen from SEs with Li for thermal runaway.

DISCUSSION

Based on the above findings, we proposed that the thermal runaway of the Ti/Ge based SEs and Li metal may be attributed to a multi-step reaction mechanism, as illustrated in Figure 4. First, interphases form after the Ti/Ge SEs contact with

metallic Li. As the temperature increases, the interfacial reactions are accelerated by the elevated temperature and intimate contact after Li melting. The increasing temperature and heat generated by the exo-thermal interfacial reactions further promote the thermal decomposition of SE, and lead to increased oxygen activity from SEs reacting highly exothermically with metallic Li. The significant amount of heat generated by this Li-oxygen reaction leads to thermal runaway. This can be further confirmed by the comparison of the calculated maximum heat generated from the SE/Li interfacial reaction and SE decomposition with the subsequent Li-oxygen reaction (Table S16). Therefore, the reactions of metallic Li with the oxygen generation from oxide SEs at elevated temperatures are the origin of the thermal runaway of SEs with metallic Li.

It should be noted that the release of oxygen from oxide cathodes has also been considered as a critical step in the thermal runaway process of commercial LIBs. O_2 gas is prone to react vigorously with organic electrolyte and flammable gases (e.g., C_2H_4, C_2H_6, etc.) produced by side reactions, generating a large amount of heat that promotes the subsequent combustion reactions and, thus, initiates the thermal runaway process. Here, we show the possibility that oxygen may be generated from SEs, which are previously believed to be chemically stable and thermally stable in a wide range of conditions. Most importantly, reactions between Li and oxygen can generate even higher amounts of heat (−1,197.460 kJ with 1 mol O_2) than the combustion of flammable gases in LIBs (−445.662 to −497.510 kJ with 1 mol O_2; Table S17). From the thermodynamics of fundamental chemical reactions, the ASSBs with Li-metal anode may potentially exhibit safety issues as LIBs with liquid electrolyte. Nonetheless, the kinetics of the thermal runaway reactions with oxygen from SEs may be significantly different. Since flammable gases are generated in liquid-electrolyte-based LIB cells before O_2 release from cathode, the gas-gas reactions in LIBs may occur much more rapidly than Li-oxygen reactions in ASSBs where gas-liquid/solid reaction has a confined or limited reaction frontier, which depends on the structure and geometry of the ASSB cells. Such characteristics of ASSBs may lead to improved safety performance of ASSBs with Li metal compared with liquid-electrolyte LIBs. Therefore, the thermal issues of SE/Li should be carefully investigated at the material, cell, and system levels in future studies of ASSBs. Given that the stability of SEs at elevated temperature is essential for thermal stability and cell safety performance, the stabilities of SE against Li metal at room and elevated temperatures should be considered for selecting SE materials for ASSBs.

Furthermore, our studies suggest future design strategies to resolve this thermal stability issue of materials. For example, a physical barrier may be a potential strategy to block the reaction between SE and Li. Our ARC test demonstrated that LLTO with Li_2CO_3 layer can be stable with metallic Li in range of 30°C–350°C (Figure S11). Moreover, the oxygen generation reactions in ASSBs largely depend on the cell architectures. The experiments from Inoue et al. indicates that rational anode-cathode design can minimize the heat generations from cathode side O_2 releasing.[15,33] Potential ASSB designs that can deliver distinct interfacial behaviors are shown in Figure S12. The influence of the battery architectures on safety performance remains unknown but should be taken into consideration in future research and development of ASSBs.

In summary, the present work is an attempt to quantify the thermal stability of several typical SEs with Li. It was found that thermal runaway occurred at interfaces between metallic Li and LAGP, LATP, and LLTO, and the high Li reactivity and the oxygen generation in oxide-based SEs was hypothesized to be the possible origin of the thermal

runaway. It is important to emphasize that our study only concerns the thermal stability of SE materials with Li, which is only one of the steps in the whole thermal runaway reaction process of ASSBs. Whether the reaction with Li is the key step for the whole thermal runaway process should be further studied for determining the key factors in the safety limits of ASSBs. Moreover, these concerns should also be taken into consideration for other systems. For example, sulfide-based electrolytes could encounter similar problems as reported here for oxide SEs, as the sulfides exhibits weaker chemical bonding than oxides. Thermal stability between sulfide-based electrolytes and Li is worthy for future investigations. Nonetheless, as an alert to the community, our results highlight the urgency to systematically investigate and deepen the understanding of safety issues in ASSBs. Further studies about the thermal stability in practical ASSBs, including different cathode/anode interfaces, Li behavior after melting point, and various battery aging states are required for the commercial realization of ASSBs.

EXPERIMENTAL PROCEDURES

Resource Availability

Lead Contact

Hong Li: hli@iphy.ac.cn

Materials Availability

Four prevalent oxide SEs were selected in our experiments. The NASICON-type LATP powder was provided by CITIC Guoan MGL, Tianjin, China. The LAGP powder was purchased from Kejing Materials Technology, Hefei, Anhui, China. The LLTO powder was provided by Tianmu Energy Anode Material and the LLZO powder was purchased from Taian Faraday Energy.

Data and Code Availability

All data in this manuscript are available by request from the Lead Contact.

Other Supplemental Experimental Procedures are detailed in Supplemental Information.

SUPPLEMENTAL INFORMATION

Supplemental Information can be found online at https://doi.org/10.1016/j.joule.2020.03.012.

ACKNOWLEDGMENTS

The work was supported by funding from the National Key R&D Program of China (grant no. 2016YFB0100100) and National Natural Science Foundation of China (grant nos. 51822211 and U1932220). A.M.N. acknowledges the support by Engie North America Chuck Edwards Memorial Fellowship. Y.M. acknowledges the support by A. James Clark School of Engineering, University of Maryland and the computational facilities from the University of Maryland supercomputing resources, and the Maryland Advanced Research Computing Center (MARCC).

AUTHOR CONTRIBUTIONS

X.Y., H.L., and Y.M. conceived the project; R.C. and J.L. prepared and performed the ARC experiments; A.M.N. and Y.M. performed and analyzed the thermodynamic calculations; J.W. carried out the post-XRD analysis; and R.C., X.Y., Y.M., A.M.N., and H.L. prepared the manuscript. All authors contributed in discussions and paper revisions of the whole manuscript.

DECLARATION OF INTERESTS

The authors declare no competing interests.

Received: January 1, 2020
Revised: January 28, 2020
Accepted: March 18, 2020
Published: April 15, 2020

REFERENCES

1. Zhang, H., Li, C., Eshetu, G.G., Laruelle, S., Grugeon, S., Zaghib, K., Julien, C., Mauger, A., Guyomard, D., Rojo, T., et al. (2020). From solid-solution electrodes and the rocking-chair concept to today's batteries. Angew. Chem. Int. Ed. Engl. *59*, 534–538.

2. Liu, B., Zhang, J., and Xu, W. (2018). Advancing Li metal batteries. Joule *2*, 833–845.

3. Cao, W., Zhang, J., and Li, H. (2020). Batteries with high theoretical energy densities. Energy Storage Mater. *26*, 46–55.

4. Kirchhoff, B. (1861). XXIV.—on chemical analysis by spectrum-observations. Q. J. Chem. Soc. *13*, 270–289.

5. Li, Y., Feng, X., Ren, D., Ouyang, M., Lu, L., and Han, X. (2019). Thermal runaway triggered by plated Li on the anode after fast charging. ACS Appl. Mater. Inter. *11*, 46839–46850.

6. Janek, J., and Zeier, W.G. (2016). A solid future for battery development. Nat. Energy *1*, 16141.

7. Xu, L., Tang, S., Cheng, Y., Wang, K., Liang, J., Liu, C., Cao, Y., Wei, F., and Mai, L. (2018). Interfaces in solid-state Li batteries. Joule *2*, 1991–2015.

8. Wang, P., Qu, W., Song, W., Chen, H., Chen, R., and Fang, D. (2019). Electro–chemo–mechanical issues at the interfaces in solid-state Li metal batteries. Adv. Funct. Mater. *29*, 1900950.

9. Yu, X., and Manthiram, A. (2018). Electrode–electrolyte interfaces in Li-based batteries. Energy Environ. Sci. *11*, 527–543.

10. Wu, B., Wang, S., Evans IV, W.J., Deng, D.Z., Yang, J., and Xiao, J. (2016). Interfacial behaviours between Li ion conductors and electrode materials in various battery systems. J. Mater. Chem. A *4*, 15266–15280.

11. Chen, R., Li, Q., Yu, X., Chen, L., and Li, H. (2019). Approaching practically accessible solid-state batteries: stability issues related to solid electrolytes and interfaces. Chem. Rev. *25*, https://doi.org/10.1021/acs.chemrev.9b00268.

12. Chung, H., and Kang, B. (2017). Mechanical and thermal failure induced by contact between a $Li_{1.5}Al_{0.5}Ge_{1.5}(PO_4)_3$ solid electrolyte and Li metal in an all solid-state Li cell. Chem. Mater. *29*, 8611–8619.

13. Lewis, J.A., Cortes, F.J.Q., Boebinger, M.G., Tippens, J., Marchese, T.S., Kondekar, N., Liu, X., Chi, M., and McDowell, M.T. (2019). Interphase morphology between a solid-state electrolyte and Li controls cell failure. ACS Energy Lett. *4*, 591–599.

14. Tippens, J., Miers, J.C., Afshar, A., Lewis, J.A., Cortes, F.J.Q., Qiao, H., Marchese, T.S., Di Leo, C.V., Saldana, C., and McDowell, M.T. (2019). Visualizing chemomechanical degradation of a solid-state battery electrolyte. ACS Energy Lett. *4*, 1475–1483.

15. Inoue, T., and Mukai, K. (2017). Are all-solid-state Li-ion batteries really safe? Verification by differential scanning calorimetry with an all-inclusive microcell. ACS Appl. Mater. Inter. *9*, 1507–1515.

16. Feng, X., Fang, M., He, X., Ouyang, M., Lu, L., Wang, H., and Zhang, M. (2014). Thermal runaway features of large format prismatic Li ion battery using extended volume accelerating rate calorimetry. J. Power Sources *255*, 294–301.

17. Feng, X., Zheng, S., Ren, D., He, X., Wang, L., Cui, H., Liu, X., Jin, C., Zhang, F., Xu, C., et al. (2019). Investigating the thermal runaway mechanisms of Li-ion batteries based on thermal analysis database. Appl. Energy *246*, 53–64.

18. Feng, X., Zheng, S., Ren, D., He, X., Wang, L., Liu, X., Li, M., and Ouyang, M. (2019). Key characteristics for thermal runaway of Li-ion batteries. Energy Procedia *158*, 4684–4689.

19. Li, Y., Chen, X., Dolocan, A., Cui, Z., Xin, S., Xue, L., Xu, H., Park, K., and Goodenough, J.B. (2018). Garnet electrolyte with an ultralow interfacial resistance for Li-metal batteries. J. Am. Chem. Soc. *140*, 6448–6455.

20. Boulant, A., Bardeau, J.F., Jouanneaux, A., Emery, J., Buzare, J.Y., and Bohnke, O. (2010). Reaction mechanisms of $Li_{0.30}La_{0.57}TiO_3$ powder with ambient air: H^+/Li^+ exchange with water and Li_2CO_3 formation. Dalton Trans. *39*, 3968–3975.

21. Huo, H., Luo, J., Thangadurai, V., Guo, X., Nan, C., and Sun, X. (2020). Li_2CO_3: a critical issue for developing solid garnet batteries. ACS Energy Lett. *5*, 252–262.

22. Dashjav, E., Ma, Q., Xu, Q., Tsai, C., Giarola, M., Mariotto, G., and Tietz, F. (2018). The influence of water on the electrical conductivity of aluminum-substituted Li titanium phosphates. Solid State Ionics *321*, 83–90.

23. Wolfenstine, J., Allen, J.L., Read, J., and Sakamoto, J. (2013). Chemical stability of cubic $Li_7La_3Zr_2O_{12}$ with molten Li at elevated temperature. J. Mater. Sci. *48*, 5846–5851.

24. Li, H., Duan, Q., Zhao, C., Huang, Z., and Wang, Q. (2019). Experimental investigation on the thermal runaway and its propagation in the large format battery module with $Li(Ni_{1/3}Co_{1/3}Mn_{1/3})O_2$ as cathode. J. Hazard. Mater. *375*, 241–254.

25. Janssen, P., Schmitz, R., Müller, R., Isken, P., Lex-Balducci, A., Schreiner, C., Winter, M., Cekić-Laković, I., and Schmitz, R. (2014). 1,3,2-Dioxathiolane-2,2-dioxide as film-forming agent for propylene carbonate based electrolytes for Li-ion batteries. Electrochim. Acta *125*, 101–106.

26. Richards, W.D., Miara, L.J., Wang, Y., Kim, J.C., and Ceder, G. (2016). Interface stability in solid-state batteries. Chem. Mater. *28*, 266–273.

27. Xiao, Y., Wang, Y., Bo, S., Kim, J.C., Miara, L.J., and Ceder, G. (2020). Understanding interface stability in solid-state batteries. Nat. Rev. Mater. *5*, 105–126.

28. Zhu, Y., He, X., and Mo, Y. (2015). Origin of outstanding stability in the Li solid electrolyte materials: insights from thermodynamic analyses based on first-principles calculations. ACS Appl. Mater. Inter. *7*, 23685–23693.

29. Ong, S.P., Jain, A., Hautier, G., Kang, B., and Ceder, G. (2010). Thermal stabilities of delithiated olivine MPO_4 (M=Fe, Mn) cathodes investigated using first principles calculations. Electrochem. Commun. *12*, 427–430.

30. Jain, A., Hautier, G., Ong, S.P., Dacek, S., and Ceder, G. (2015). Relating voltage and thermal safety in Li-ion battery cathodes: a high-throughput computational study. Phys. Chem. Chem. Phys. *17*, 5942–5953.

31. Ong, S.P., Wang, L., Kang, B., and Ceder, G. (2008). $Li-Fe-P-O_2$ phase diagram from first principles calculations. Chem. Mater. *20*, 1798–1807.

32. Liu, X., Ren, D., Hsu, H., Feng, X., Xu, G., Zhuang, M., Gao, H., Lu, L., Han, X., Chu, Z., et al. (2018). Thermal runaway of Li-ion batteries without internal short circuit. Joule *2*, 2047–2064.

33. Uyama, T., Inoue, T., and Mukai, K. (2018). Realizing the ultimate thermal stability of a Li-ion battery using two zero-strain insertion materials. ACS Appl. Energy Mater. *1*, 5712–5717.